Electroactive micro and nanowells for optofluidic storage

Bernardo Cordovez,[1] Demetri Psaltis,[2,3] and David Erickson[1,*]

[1]*Sibley School of Mechanical and Aerospace Engineering, Cornell University, Ithaca, NY, 14853, USA*
[2]*School of Engineering, École Polytechnique Fédérale de Lausanne (EPFL), Switzerland*
[3]*Department of Electrical Engineering, California Institute of Technology, Pasadena, CA, 91125, USA*
**de54@cornell.edu*

Abstract: This paper reports an optofluidic architecture which enables reversible trapping, detection and long term storage of spectrally multiplexed semiconductor quantum dot cocktails in electrokinetically active wells ranging in size from 200nm to 5μm. Here we describe the microfluidic delivery of these cocktails, fabrication method and principal of operation for the wells, and characterize the readout capabilities, storage and erasure speeds, internal spatial signal uniformity and potential storage density of the devices. We report storage and erase speeds of less than 153ms and 30ms respectively and the ability to provide 6-bit storage in a single 200nm well through spectral and intensity multiplexing. Furthermore, we present a novel method for enabling passive long term storage of the quantum dots in the wells by transporting them through an agarose gel matrix. We envision that this technique could find eventual application in fluidic memory or display devices.

OCIS codes: (250.5590) Quantum-well, -wire and -dot devices; (210.4680) Optical memories; (260.2510) Fluorescence.

References and links

1. I. Vlassiouk, and Z. S. Siwy, "Nanofluidic diode," Nano Lett. **7**(3), 552–556 (2007).
2. T. Thorsen, S. J. Maerkl, and S. R. Quake, "Microfluidic large-scale integration," Science **298**(5593), 580–584 (2002).
3. A. Groisman, M. Enzelberger, and S. R. Quake, "Microfluidic memory and control devices," Science **300**(5621), 955–958 (2003).
4. M. Prakash, and N. Gershenfeld, "Microfluidic bubble logic," Science **315**(5813), 832–835 (2007).
5. E. Betzig, J. K. Trautman, R. Wolfe, E. M. Gyorgy, P. L. Finn, M. H. Kryder, and C. H. Chang, "Near-Field Magnetooptics and High-Density Data-Storage," Appl. Phys. Lett. **61**(2), 142–144 (1992).
6. L. Dhar, K. Curtis, and T. Facke, "Holographic data storage: Coming of age," Nat. Photonics **2**(7), 403–405 (2008).
7. H. J. Coufal, D. Psaltis, and G. Sincerbox, *Holographic data storage* (Springer, Berlin, 2000).
8. X. Zhang, and Z. W. Liu, "Superlenses to overcome the diffraction limit," Nat. Mater. **7**(6), 435–441 (2008).
9. D. Burgreen, and F. R. Nakache, "Electrokinetic flow in ultrafine capillary slits," J. Phys. Chem. **68**(5), 1084–1091 (1964).
10. D. Erickson, T. Rockwood, T. Emery, A. Scherer, and D. Psaltis, "Nanofluidic tuning of photonic crystal circuits," Opt. Lett. **31**(1), 59–61 (2006).
11. M. Y. Gao, J. Q. Sun, E. Dulkeith, N. Gaponik, U. Lemmer, and J. Feldmann, "Lateral patterning of CdTe nanocrystal films by the electric field directed layer-by-layer assembly method," Langmuir **18**(10), 4098–4102 (2002).
12. Q. Sun, Y. A. Wang, L. S. Li, D. Y. Wang, T. Zhu, J. Xu, C. H. Yang, and Y. F. Li, "Bright, multicoloured light-emitting diodes based on quantum dots," Nat. Photonics **1**(12), 717–722 (2007).
13. J. Heikenfeld, K. Zhou, E. Kreit, B. Raj, S. Yang, B. Sun, A. Milarcik, L. Clapp, and R. Schwartz, "Electrofluidic displays using Young-Laplace transposition of brilliant pigment dispersions," Nat. Photonics **3**(5), 292–296 (2009).
14. A. C. Siegel, S. T. Phillips, B. J. Wiley, and G. M. Whitesides, "Thin, lightweight, foldable thermochromic displays on paper," Lab Chip **9**(19), 2775 (2009).

#113847 - $15.00 USD Received 7 Jul 2009; revised 28 Oct 2009; accepted 28 Oct 2009; published 5 Nov 2009

15. J. Li, Q. Zhang, N. Peng, and Q. Zhu, "Manipulation of carbon nanotubes using AC dielectrophoresis," Appl. Phys. Lett. **86**(15), 153116 (2005).
16. M. L. Y. Sin, V. Gau, J. C. Liao, D. A. Haake, and P. K. Wong, "Active Manipulation of Quantum Dots using AC Electrokinetics," J. Phys. Chem. C **113**(16), 6561–6565 (2009).
17. D. Psaltis, S. R. Quake, and C. Yang, "Developing optofluidic technology through the fusion of microfluidics and optics," Nature **442**(7101), 381–386 (2006).
18. C. Monat, P. Domachuk, and B. J. Eggleton, "Integrated optofluidics: A new river of light," Nat. Photonics **1**(2), 106–114 (2007).
19. B. Cordovez, D. Psaltis, and D. Erickson, "Trapping and storage of particles in electroactive microwells," Appl. Phys. Lett. **90**(2), 024102 (2007).
20. A. K. Gooding, D. E. Gómez, and P. Mulvaney, "The effects of electron and hole injection on the photoluminescence of CdSe/CdS/ZnS nanocrystal monolayers," ACS Nano **2**(4), 669–676 (2008).
21. M. Bruchez, Jr., M. Moronne, P. Gin, S. Weiss, and A. P. Alivisatos, "Semiconductor nanocrystals as fluorescent biological labels," Science **281**(5385), 2013–2016 (1998).
22. D. Erickson, "Spectrographic microfluidic memory," in *Proc. ICMM*(Canada, 2005).
23. M. Y. Han, X. H. Gao, J. Z. Su, and S. Nie, "Quantum-dot-tagged microbeads for multiplexed optical coding of biomolecules," Nat. Biotechnol. **19**(7), 631–635 (2001).
24. S. Chang, M. Zhou, and C. Grover, "Information coding and retrieving using fluorescent semiconductor nanocrystals for object identification," Opt. Express **12**(1), 143–148 (2004).
25. M. Mansuripur, A. R. Zakharian, A. Lesuffleur, S.-H. Oh, R. J. Jones, N. C. Lindquist, H. Im, A. Kobyakov, and J. V. Moloney, "Plasmonic nano-structures for optical data storage," Opt. Express **17**(16), 14001–14014 (2009).
26. P. Zijlstra, J. W. M. Chon, and M. Gu, "Five-dimensional optical recording mediated by surface plasmons in gold nanorods," Nature **459**(7245), 410–413 (2009).
27. C. Chen, S. L. Liu, R. Cui, B. H. Huang, Z. Q. Tian, P. Jiang, D. W. Pang, and Z. L. Zhang, "Diffusion Behaviors of Water-Soluble CdSe/ZnS Core/Shell Quantum Dots Investigated by Single-Particle Tracking," J. Phys. Chem. C **112**, 18904–18910 (2008).
28. J. Narayanan, J.-Y. Xiong, and X.-Y. Liu, "Determination of agarose gel pore size: Absorbance measurements vis a vis other techniques," Journal of Physics: Conference Series **28**, 83–86 (2006).

1. Introduction

Recent advances in micro- and nano-fluidics has rekindled an interest in fluid based optoelectronic [1] devices. Within this larger field, several fluidic data storage and logic devices have been recently demonstrated, including that by Thorsen *et al.* [2] where a microfluidic device was used to create an array of discrete chambers which could be probed for the presence of a dye, that by Groisman *et al.* [3] which exploited viscoelastic polymer solutions to create fluidic flip-flops, and that by Prakash *et al.* [4] in which microfluidic bubbles where used to generate an array of universal Boolean logic components. Although these devices have some practical benefits over traditional devices (for example ruggedness to electromagnetic radiation), the fundamental advantage is that they allow the integration of chemical and biological reactions into the logic operation. The main drawbacks of these devices is that the density with which the operations can be stored (on the order of 50 Bs/cm^2) is extremely low compared with the state of the art data storage devices [5–8] and the speed with which they operate is currently much slower than state-of-the-art electronics or photonics. While downscaling the fluidic features is the most obvious path to addressing the first of these concerns, the extreme transport speed limitations [9] of nanofluidic devices makes further reduces the speed with which such devices can operate. For example Erickson *et al.* demonstrated the ability to tune the optical output of photonic crystals using nanochannels on the order of 300nm, however they reported very slow switching times limited by the fact that average flow velocity in a nanochannel scales with the square of the channel diameter [10].

Another area of growing research interest is that of visual display technologies. Nanocrystal based displays [11,12] are being explored due to the unique optical properties of Quantum Dots (QDots) which include ultra sharp colors (narrow emission line-width) and high quantum efficiency (brightness). Electrofluidic techniques which manipulate custom water dispersed pigments [13] have also been recently used to generate reflective pixels. In another example, Siegel *et al.* [14] demonstrated a disposable, one time use paper based thermochromic display. Consequently, it can be of great interest to establish a technique that

#113847 - $15.00 USD Received 7 Jul 2009; revised 28 Oct 2009; accepted 28 Oct 2009; published 5 Nov 2009

is able to exploit the reconfigurability of fluidic based display systems while harnessing the exceptional optical properties of QDots.

Though techniques like dielectrophoresis (DEP) [15] have been used to orient nanoscaled objects and elaborate hybrid electrokinetic techniques [16] have been employed to fluidically direct QDots, the speeds, volume precision and storage density are still below that required to compete with other technologies described above. As a potential approach to addressing this problem, we present here an optofluidic [17,18] approach for trapping QDots in discrete micro- and nanoscale locations using electrokinetically active wells. In this work we demonstrate the principal of operation for the wells on both the micro- (5μm) and nanoscale (200nm), and experimentally characterize for the first time: the potential storage density through spectral and intensity multiplexing, the storage and erasure speeds, and the internal spatial signal uniformity. We also present a novel method for enabling passive long term non-volatile of the quantum dots packets by storing them in wells containing an agarose gel matrix. In the first section below we describe the principal of operation of the device and then apply it to 200nm wells and 5μm wells in sections 3 and 4 respectively. In section 5 we characterize the write and erase times of the device. Finally section 6 describes the non-volatile storage technique.

2. Principle of Operation

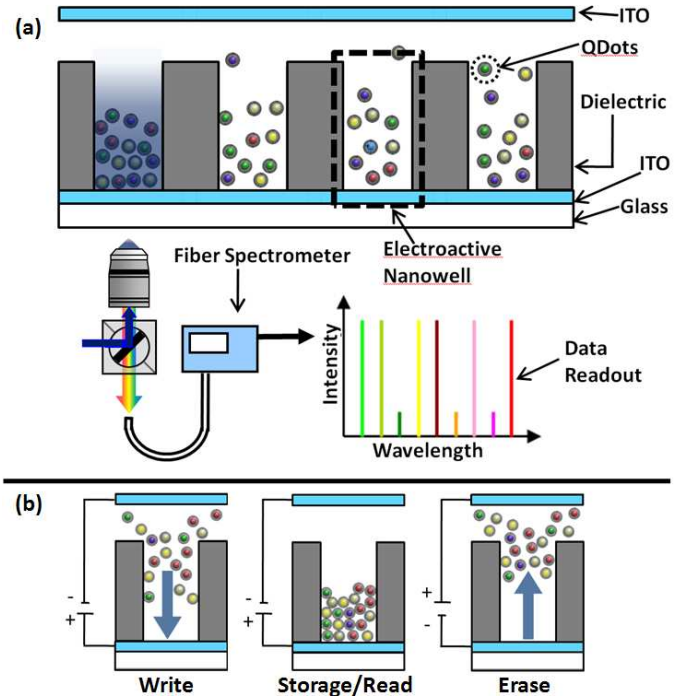

Fig. 1. Optofluidic Storage of Quantum Dots in Electrokinetically Active Micro- and Nanowells. (Media 1) (a) Quantum Dot (Q Dot) cocktails are delivered by pressure driven flow to an array of electrokinetically active 200nm diameter nanowells. During writing an electrokinetic attraction voltage is applied between the upper surface and the bottom of the nanowell which attracts the QDots into a well as shown in (b). During reading the QDots are optically excited and their emission signal is captured through a fiber spectrometer. (b) Erasing is done simply by reversing the polarity and rejecting the code from the well.

Figure 1 shows an overview of our optofluidic storage device, also available in video format in the Supplemental Information as Media 1. In the experiments performed here, the QDot storage "packets" are created by mixing solutions of different concentrations of different sized QDots with different fluorescent emission spectra. Since the solution phase concentrations of

#113847 - $15.00 USD Received 7 Jul 2009; revised 28 Oct 2009; accepted 28 Oct 2009; published 5 Nov 2009

these QDots maps directly to emission intensity, each unique combination of species at varying concentrations can be related to a unique spectral signal. Once created, the QDot data packet is delivered to an electroactive well site into which it is stored, by applying an electrical potential between the top and bottom electrodes as is displayed in Fig. 1(b). This approach avoids the transport speed limitations of nanofluidic devices by performing the long distance transport in microscale channels and the final storage step only at the nanoscale. To read out the contents of a well, the well is excited using a UV-blue light source and the fluorescent signal collected on a fiber spectrometer. Well depletion can be achieved by reversing the polarity of the field and ejecting the QDots from the wells and into the bulk fluid, then carried downstream by pressure driven flow. Details on the fabrication procedure are provided in Section 8.

3. Quantum Dot Trapping, Storage and Detection in Nanowell Geometries

In this section we demonstrate the operation of the electroactive nanowell storage elements, as can be observed in Fig. 2. The wells used in this here are 200nm in diameter and thus consistent with the size of diffraction limited data pits used in traditional planar optical storage media. Figure 2(a) shows the nanowell during electrokinetic attraction, showing a strong emission signal due to QDot accumulation in the base of the well. When the polarity is reversed [as shown in Fig. 2(b)] the QDots are repulsed from the well and the emission intensity decreases. Figure 2(c) shows an optical image of a small portion of the electroactive nanowell array and Fig. 2(d) displays an SEM of the nanowell geometry. Because we primarily focus on demonstrating the fundamental storage element, we spaced the wells relatively far apart but note that current lithographic techniques allow for denser bit packing. The repulsion state, Fig. 2(b), shows small background fluorescence, possibly due to particle adhesion, however this can be ameliorated by employing a lower attraction potential and better surface treatments [19].

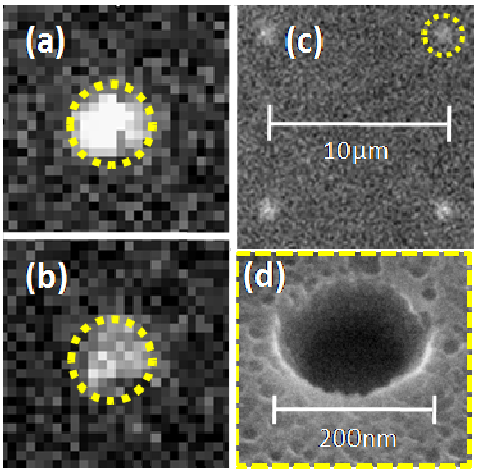

Fig. 2. Electroactive Nanowells during (a) Electrokinetic Attraction of 4nM solution of 655nm Qdots by applying a 0.8V potential. (b) Repulsion Mode (c) Optical close up of a 2x2 section of the electroactive nanowell array. (Media 2) The top right well is the one shown in (a) and (b). (d) SEM of the 200nm diameter electroactive well, 1μm in depth.

The attraction and repulsion sequences displayed in Fig. 2 can be viewed real time in video Media 2 included in the online supplementary material. Since the colloidal QDots are tagged with Streptavidin (pI ~5) they support a net negative electrophoretic mobility in this solution. For the experiments shown above we used a 4nM solution of QDots with a central emission wavelength of 655nm immersed in a 10mM phosphate buffer solution at stabilizing

#113847 - $15.00 USD Received 7 Jul 2009; revised 28 Oct 2009; accepted 28 Oct 2009; published 5 Nov 2009

pH of 8.3, under an applied electric potential of ± 0.8V and a mean channel flow velocity of 10μm/s.

Figure 3(a) shows a set of four spectrographic codes obtained from the nanowells. We demonstrate the potential for storing spectrally multiplexed QDot based memory codes by varying the concentration of the 525nm emitting species while keeping the 605nm and 705nm species unchanged. As shown, the peak intensity level of a given species varies approximately linearly with concentration. The intensity of the signals obtained is quite large mainly owing to the high aspect ratio (roughly 5:1) of the nanowells, allowing significant accumulation of QDots in the traps. The large fluorescent signal is also evidence of the strong trapping potentials in these devices [19].

Quantifying the above, in Fig. 3(b) we observe that the intensity counts increase sharply when the attraction potential is applied and similarly decrease sharply when polarity is switched, coinciding with attraction and repulsion of the QDots from the storage sites. We will return to this plot in Section 5 to analyze the temporal performance of the devices. Importantly, it can be noted in Fig. 3(b) that that the signal degrades from one electrokinetic attraction cycle to the next. This undesirable signal decay is likely due to two effects: The first is that under an applied stimulus (electric potential in our case), charge carriers can be trapped in the QDot matrix, forcing the system out of a light emitting state. Particularly, Gooding *et al*. [20] demonstrated that under a 1 V positive potential (very close to the electric condition inside our wells) and in an acetonitrile electrolyte, the photoluminescence of Cd/Se nanofilms with ZnS shells (similar composition to our QDots) irreversibly quenches with no recovery upon reversal of the electric potential. However, they did not observe this adverse effect for negative potentials. As such we will use QDots tagged with positively charged biomolecules in aqueous pH, or even raise the pH of our current buffer to see if this effect is reduced in future experiments. Moreover, the presence of an electrolytic reaction at the ITO electrode in the repulsion phase can occur at moderate potentials, lightly charring (darkening) the electrode's surface after every attraction cycle. This could be minimized by using a lower concentration buffer and smaller attraction voltage (both of which serve to reduce the rate of electrolysis), though the latter of these will slow down the temporal performance of the device. Although this represents a limitation of our current approach to nanoscale storage, as will be expanded on in the next section, we have been able to minimize this effect in larger wells.

Since the QDot storage is done in diffraction limited site and the spectral encoding allows for the storage of a large number of signals per well, this device could find use in high density storage applications. QDots are ideal for data storage due to their small size, their narrow emission line-width, their resistance to photobleaching and the ability to excite all species with a UV-blue light source [21]. We note that since this paper focuses is on the nanofluidic manipulation and trapping of QDots in electroactive nanowells, the QDot solutions employed here were generated manually. An automated spectral code writer [17,22] for discrete QDot cocktail generation was presented in an earlier publication. To demonstrate the potential use of the device in binary storage applications, consider Eq. (1) which describes the equivalent number of bits (*N)* in a single QDot cocktail information packet is given by:

$$N = \log_2\left(I^M - 1\right) \tag{1}$$

where I is the number of intensity levels and M is the number of individual species. In the experiment shown in Fig. 3(a), we show 3 separate species and 4 different intensity levels yielding $N = 6$ separate bits or a 6 fold increase over current single bit media. Existing commercially available QDots exhibit emission spectral with full width half maximums on the order of 50nm and thus we expect that this approach could sense up to 8 different species emitting from the visible to the IR. If $I = M = 8$, one could read up to 24 bits in a single diffraction limited data site and hence the potential for over an order of magnitude density

#113847 - $15.00 USD Received 7 Jul 2009; revised 28 Oct 2009; accepted 28 Oct 2009; published 5 Nov 2009

increase from current surface optical storage technologies. We note that the optofluidic method demonstrated here avoids the tip-to-sample separation problem inherent in near-field and superlensing techniques (which has to be on the order of 10nm due to the exponential decay of the evanescent wave) that have been used in the past to achieve sub diffraction limited data storage [5,8]. We note that similar QDot optical encoding has previously been demonstrated for biomolecule sequencing [23]and barcoding [24], however this represents the first application directly to data storage. In this demonstration, low nanomolar concentrations helped to reduce the amount of crosstalk between adjacent bits, and note that with greater control over QDot synthesis the number of detectable species could be further increased.

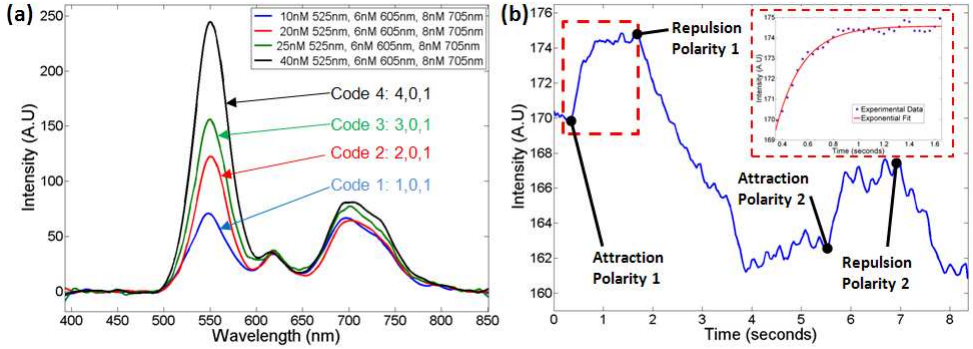

Fig. 3. (a) Spectrographic readout of simple QDot packets from the electroactive nanowells. Four different codes are shown each consisting of a combination of quantum dot with a central emission wavelength of 525m, 605nm and 705nm. The concentration of the 605nm species was increased in equal amounts from 10nM to 40nM, while the 605nm and 705nm species were held constant. After reading and erasing each bit, it is flushed and the next bit solution is introduced for data readout. (b) Mean fluorescent excitation history in electroactive nanowell during two attraction/storage/repulsion steps. The marks indicate the time in which the polarity of the applied field is switched. Inset shows the fit to the equation $a(1-exp(-t/\tau))$.

4. Extension of Electroactive Well Trapping Technique to Micrometer Scale Geometries

In the next set of experiments we analyze the reversible QDot trapping in 5μm sized electroactive wells in order to demonstrate the applicability of the technique across a range of scales and to examine the spatial uniformity of the quantum dot distribution in the wells. The primary advantage of larger wells is that the ratio of the well base to the volume of the attraction basin is larger and thus the signal to background ratio can be higher. While the spatial density might be too low for memory applications, larger wells could find an application as a fast and spatially uniform technique for pixel writing in nanocrystal displays [11,12]. Figure 4(a) shows the 5 μm microwell during electrokinetic attraction. Figure 4(b) shows the decrease in fluorescent intensity after reversing the polarity of the applied field. The attraction and repulsion sequences displayed in Fig. 4 can be viewed real time in Media 3. included in the online supplementary material. Figure 9 and Fig. 10 in the supplementary section show the corresponding spectrographic readouts and intensity vs. time trace for this size well. In Fig. 4(c) we present the spatial uniformity of the QDot emission from inside the large microwell. As can be seen, the emission intensity remains relatively flat along most of the radius of the well but begins to drop off towards the edge. In our previous work we have shown that electroosmotic transport leads to recirculation inside the walls of the electroactive wells [19], resulting in increased accumulation of particles on the well edges. However, in Fig. 4(c) it can be appreciated that since the emission is spatially uniform except near the edges, the dominant transport effect is electrophoresis rather than electroosmosis. This is expected since the moderately high buffer concentration strongly suppresses the Debye layer, thus diminishing electroosmotic effects. For display applications, this will minimize localized QDot clustering at the well edges leading to a more uniform distribution.

#113847 - $15.00 USD Received 7 Jul 2009; revised 28 Oct 2009; accepted 28 Oct 2009; published 5 Nov 2009

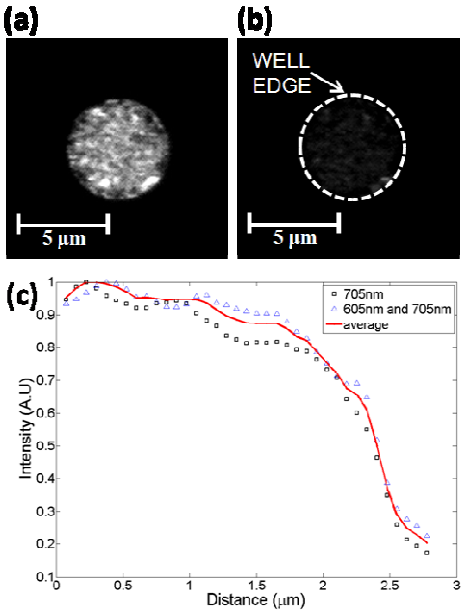

Fig. 4. Large electroactive microwell during (a-b) Attraction and rejection of a mixture containing 3 nM 705nm with 6nM 605nm emitting QDots (c) Radial distribution of fluorescent intensity inside microwell. The cocktail used here contained 3 nM 705nm with 6nM 605nm emitting QDots at pH = 8.3. This solution was delivered to the well at an average flow speed of 40µm/s and then trapped by applying a 0.8V potential (Media 3).

5. Device Temporal Characterization and Well Spatial Density Analysis

In this section we characterize the trapping (or write) and repulsion (or erase) time scales as a function of the flow conditions and well dimensions. To do this, the average intensity from the wells during the attraction phase was fit to an exponential relation $a(1-exp(-t/\tau))$. A sample fit is shown in the inset of Fig. 3(b), where a is a fitting parameter, t is the elapsed time and τ is the characteristic time constant for well filling saturation. This was used as the parameter to characterize write speed of the device. For an attraction voltage of 0.8V, the smallest time constant achieved for the nanowells was 153ms at a mean flow speed of 43µm/s. Plotting the measured time constants as a function of the transport velocity in Fig. 5 shows a decreasing trend in the time constant with increasing flow speed. A linear fit to the data shows that for every increase of 1 µm/s in average channel velocity, the trapping time constant decreases by 7 ms. As such the write speed could be significantly improved by increasing the transport flow velocity. The reason the writing speed increases with velocity is that the mass flux of entering the attraction basin of a given well increases. For the larger wells (see inset in Fig. 5) the trapping time is longer but the dependence on flow speed is much higher. This is because the attraction basin of the larger wells is bigger and thus is more effective in attracting nanoparticles from farther away. The smallest erase time scale recorded was measured to be less than 30ms, (see Fig. 10).

#113847 - $15.00 USD Received 7 Jul 2009; revised 28 Oct 2009; accepted 28 Oct 2009; published 5 Nov 2009

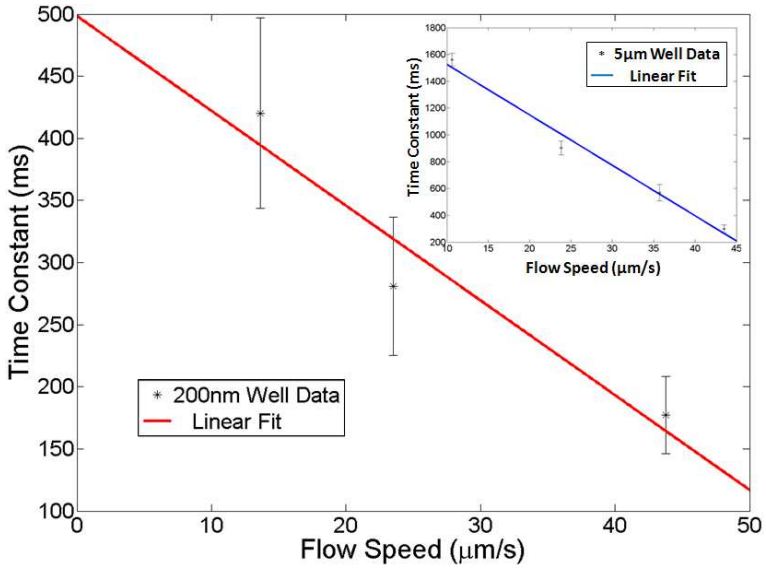

Fig. 5. Attraction time scales vs. mean channel velocity. The time scale data was obtained by performing exponential fits to the time intensity data. The red linear fit is made for the 200nm electroactive well data while the blue linear fit in the inset displays the trend for the 5 μm well data.

It is important to note that there have been many important advancements using nanoparticles in optical data storage, particularly focusing on exploiting surface plasmon interactions in metallic nanorods to multiplex in the wavelength, polarization and spatial domains [25,26]. While these devices potentially offer higher storage densities and very fast data storage and retrieval, our device enables multiplexing while also permitting data to be rewritten and does not require expensive pulsed laser setups. Furthermore, while the reported serial write time for our device of 40 bit/second is much lower than other storage devices, it is important to note that one of the key attributes of our device is that it enables simultaneous data as well as chemical storage. It can therefore serve as an interface between large scale chemical and biological integration and computation. In this respect, it is important to consider the time scales involved in traditional biochemical sensing platforms as well. For example, a reliable DNA chip test can take on the order of days (~105 s) due to its diffusion limited transport. Our device is capable of transferring material on the order of 10^{-1} s which lies roughly halfway between the above and that for established pure data storage techniques (~10-8 s). The reported write time also allows us to place limits on the theoretical highest achievable bit density that does not exhibit diffusion based cross talk between neighboring storage. Given our current 150ms write time, a first order calculation using Fick's diffusion length, $L_{space} = (4Dt)^{1/2}$, using the diffusion coefficients, D, reported in Chen *et al.* [27] leads to L_{space} = 770nm which is roughly twice the minimum blu-ray pitch (320nm). With our demonstrated factor of 6 improvement, this gives us a 1.5 fold increase in storage density over single layer blu-ray using physical matter. By decreasing the write time to 25ms or increasing the storage density to 24-bit/well a 6 fold improvement would be possible.

6. Non-Volatile Storage Using an Agarose Gel Matrix

Both the micro- and nanoscale storage devices described above are volatile in that an external voltage needs to be continuously applied to sustain QDot retention. Without this applied electric potential, QDots will diffuse out of the well and the fluorescence signal is lost in a relatively short time. In order to extend this signal retention, we coated the microwells with a thin agarose hydrogel which will inhibit nanoparticle diffusion. Figure 6(a) shows the

#113847 - $15.00 USD Received 7 Jul 2009; revised 28 Oct 2009; accepted 28 Oct 2009; published 5 Nov 2009

nonvolatile device operation schematic. As before, QDot cocktails are fluidically delivered to the vicinity of an agarose coated electrokinetic well. The electric potential is then applied between the top and bottom ITO electrodes, generating a confined electric field inside the microwell. The resulting electrokinetic forces drive the particles inside the wells through the nanoscale pores in the agarose gel. Figure 6(b) displays an SEM illustrating a gel covered well; with a pore size near 200nm for a 1% weight by volume (roughly matching the results of Narayan *et al.* [28]. An SEM of the cross section of the well geometry can be found in Fig. 11. As will be shown below, just like in the uncoated scenario, the wells can be depleted by reversing the polarity and ejecting the QDots to the bulk fluid. Such a coating was easier to employ in the microwell geometries, which is why this technique was not used in the nanowell case.

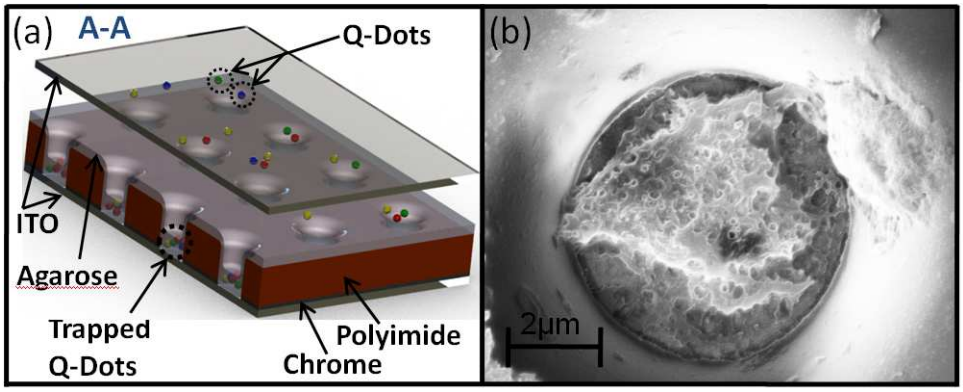

Fig. 6. (a) Non-volatile storage device schematic (x-section view). QDots are trapped in the wells and through the nanoscale pores of the gel (b) SEM of gel covered microwell for a 1% w/v coating.

Figure 7 illustrates how the mean fluorescent intensity varies for attraction and repulsion sequences at various gel concentrations (and therefore pore sizes). Just like in the nanoscale wells, the attraction setting results in the localization of the QDots inside the wells and is observed as an increase in mean fluorescent intensity and the opposite occurs for electrokinetic repulsion. These characteristic time scales of these processes are also presented in Table 1.

Table 1. Time Scale Summary of Microwell Traps

Agarose [%w/v]	Pore Size[a] [nm]	Attraction [ms]	Repulsion [ms]	Retention [sec]
0	N/A	343 (± 38)	193 (± 35)	178 (± 35)
0.5	~500	434 (± 58)	215 (± 46)	3752 (± 524)
1	~200	405 (± 82)	226 (± 79)	3120 (± 784)
1.5	~100	822(± 157)	391 (± 92)	>5000 [b]

[a]From Narayan *et al.* Reference [25]
[b]Photo -Bleaching Limited

The first result here is that for gel concentrations varying from 0 to 1% w/v, though the attraction and repulsion times tend to increase (slower response) with decreasing pore size, the overall change is not great. The similar time scales likely result due to the fact that since even for the smaller pores at 1% (~200nm when fully hydrated) this is still at least ten times greater in size than a QDot diameter. Furthermore, the sizes of the pores are also large enough so that Debye Layer proximity (for this 1mM solution the Debye length is on the order of 10nm) will not result in significant flow retardation. However, during the overnight gel dehydration process (explained in the Experimental Section) at the increased 1.5% w/v setting, the result is likely unstable pore formation, leading to their shrinking and collapsing. Thus, the attraction

#113847 - $15.00 USD Received 7 Jul 2009; revised 28 Oct 2009; accepted 28 Oct 2009; published 5 Nov 2009

process is roughly 2.4 times slower for the high sugar concentration scenario when compared to the rest. It will be noted below, however, that the signal retention time under no external voltage will be greatly enhanced for this same gel concentration. As is also shown in Fig. 7, for gels with agarose concentrations 1%w/v and below, the attraction and repulsion processes are almost entirely reversible. At the 1.5%w/v scenario, it was found that there was heavy non specific adsorption of the QDots onto the gel, which is manifested as a fluorescent accumulation between attraction and repulsion cycles. Though treating this gel type with surfactants may be of interest to reduce this accumulation, our results indicate here the gel is becoming effectively saturated and solidified.

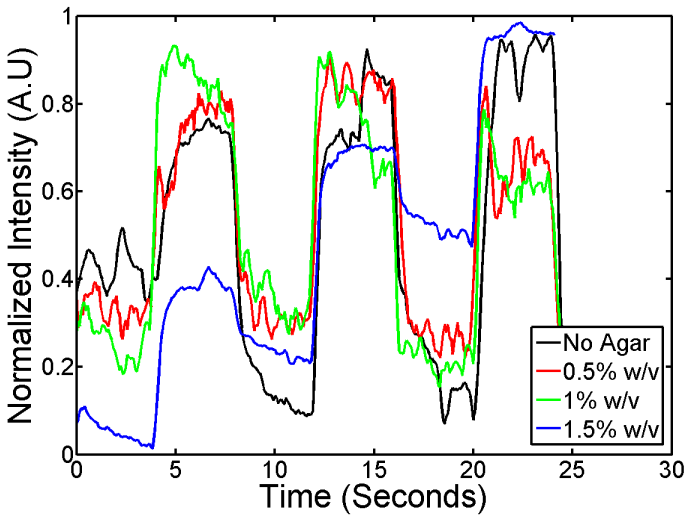

Fig. 7. Mean fluorescent excitation history in an electroactive microwell with gel coatings at various agarose concentrations during a sequence of attraction and repulsion steps.

Figure 8 illustrates the how the QDot retention varies as a function of pore size. In this experiment, the particles are delivered to the well sites, and after 3 minutes, a 1V attraction potential is applied and immediately turned off. For the uncoated scenario, the QDot diffusion out of the well effectively depletes the fluorescent intensity in less than three minutes, making this scenario less useful for long term storage at lower power cost. The retention time scales, here defined as the time it takes the fluorescent signal to decay to half of its fully saturated value, are also shown in Table 1. For the 0.5% and 1% w/v, similar retention times on the order of an hour were observed, representing nearly a twenty-fold increase over the uncoated case. For the 1.5% w/v case, retention times were typically greater than 5000s. As mentioned before, this scenario offers the best retention characteristics, but exhibits a slower electrokinetic response and also suffers from undesirable nonspecific adsorption.

#113847 - $15.00 USD Received 7 Jul 2009; revised 28 Oct 2009; accepted 28 Oct 2009; published 5 Nov 2009

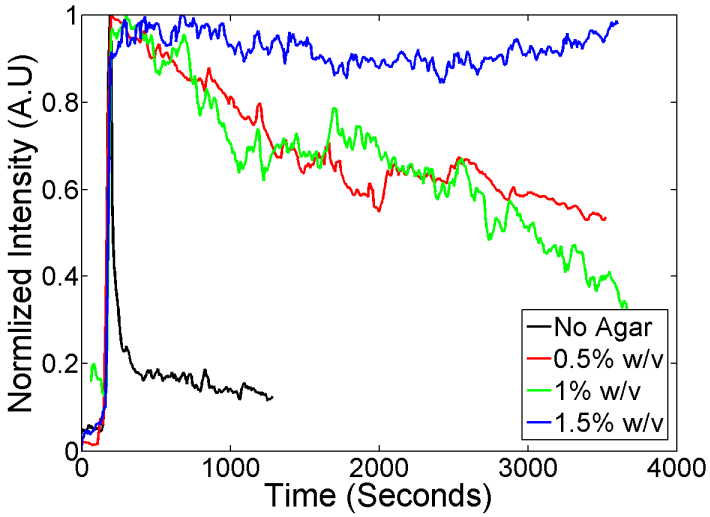

Fig. 8. Fluorescent signal retention history as in an electroactive microwell with gel coatings at various agarose concentrations. A 1V potential is applied at the 180 second mark and instantaneously switched off.

7. Outlook and Conclusions

In summary, we have demonstrated and characterized here a new micro- and nanofluidic approach to physical storage of spectrally and intensity multiplexed Quantum Dot packets. In addition to introducing the devices, we show the potential for exceeding the storage limits of single-layer diffraction limited optical storage media by between 1.5 and 6 fold, and report data read and erase times of 153 and under 30 milliseconds respectively. We also demonstrate and characterize a technique for enabling non-volatile storage of the Q-Dot packets using an agarose gel matrix. With this technique, passive retention times greater than 1hr are demonstrated.

We focused here on demonstrating the important basic storage element and the potential behind the technology, however in order to create a fully integrated device there are several future technical challenges which must be addressed. Among the most important of these are continuous rewritability and individual well addressability. An integrated device must achieve continuous rewriteability in that after a data cocktail is erased, one must break the data packet of interest into its basic units so that it can be returned to the spectral code writer [17,22]. We show how this could be accomplished in Fig. 12 where an initially homogeneous data packet is separated into its constituent red, yellow and green colors using electrophoresis since the smaller sized quantum dots migrate faster downstream than the larger ones. With regards to the second challenge, although electrical addressability on the scale of that required here to address individual arrays of 200nm diameter wells is well within the fabrication limits of current CMOS technology, additional complications are expected such as device alignment and inter-well electrical cross talk. In future versions of the device we hope to address some of these concerns.

8. Materials and Methods

8.1 Electroactive Nano and Microwell Fabrication

A thin 8-12 ohm ITO coated coverslip (SPI Supplies) was coated with a 40nm chrome layer, a 200nm thin oxide stop layer, a 600nm silicon body and a 280nm oxide mask. Wells 200nm in diameter were patterned on the substrate with PMMA (Polymethyl methacrylate)) based resist through electron beam lithography, followed by a sequence of reactive ion etches and a final

#113847 - $15.00 USD Received 7 Jul 2009; revised 28 Oct 2009; accepted 28 Oct 2009; published 5 Nov 2009

wet chrome etch, leaving the ITO layer exposed. ITO was chosen as the bottom transparent conductor in order to enable fluorescent excitation from below the substrate [21]. Additional details of the fabrication can be found in the Supporting Information under Electroactive Nanowells Fabrication.pdf, Media 4.

Though the same technique can be used to pattern the larger sized wells, a simpler fabrication technique as shown in Fig. 6. Electrically active microwells (5 µm radius by 5 µm tall) where fabricated on top of an ITO coverslip and a 100nm chrome layer by using spin on positive photoactive polyimide (HD MicroSystems 8820). The microwells were patterned and developed, followed by a quick chrome etch, which results in clear, conductive wells surrounded by an opaque layer which blocks polyimide self fluorescence during irradiation. We note that the silicon/oxide and polyimide based dielectrics did not lead to changes in the QDot transport and both served as good insulators.

8.2 Non Specific Adsorption Treatment, QDot Solutions and Agarose Coating Preparation

After well fabrication, the substrate was cleaned with oxygen plasma, and left overnight at room temperature shaking in a 5ml toluene solution containing 50 µl PEG (Polyethylene Glycol) - Silane, and 50 µl of a Triethylamine catalyzer. The chip was then rinsed in toluene and baked at 80°C for 2 hours to polymerize the PEG silane. Discrete nanocrystal cocktails were created by mixing different nanomolar concentrations of different species of Streptavidin (pI~5) modified CdSe (ZnS shell) QDots (Invitrogen Corp.) in a 1mM solution of DI water solution of pH = 8.3. Since we focus here on the data storage challenges, the QDot solutions employed were generated manually and offline. A QDot spectral code writer for active QDot mixing was presented in an earlier paper [17,22]. It is important to note that fluorescent excitation was not performed with a regular UV-Blue QDot filter, but with a green (525nm) excitation filter instead. This served to help reduce any potential bleaching of the already robust QDots.

Using a high melting temperature gel 70°C (Omnipur), thin agarose gel membranes where prepared by mixing different solution phase concentrations of agarose (0.5%, 1% and 1.5% w/v) with 1mM DI water at pH = 8.3 followed by heating to 120°C for 20 minutes. 5 µl of the heated solution was pipetted on top of the wells and left at room temperature overnight, resulting in a thin and nearly uniform membrane measuring from 2.5 to 3µm on top of the wells.

#113847 - $15.00 USD Received 7 Jul 2009; revised 28 Oct 2009; accepted 28 Oct 2009; published 5 Nov 2009

9. Supplementary Figures

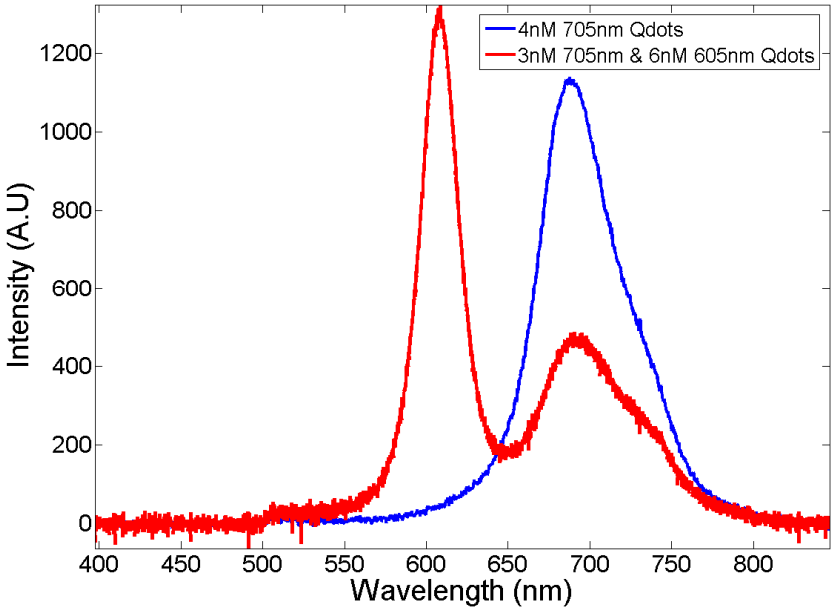

Fig. 9. Spectrographic Code read in electroactive microwell setting shown in Fig. 4(a).

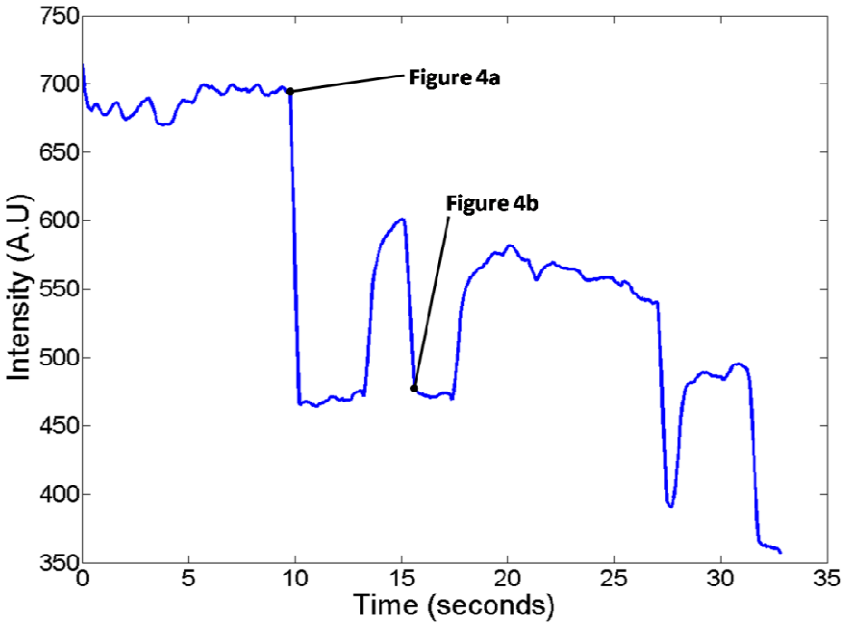

Fig. 10. Mean fluorescent intensity vs. time trace for electroactive microwell shown in Fig. 4.

#113847 - $15.00 USD Received 7 Jul 2009; revised 28 Oct 2009; accepted 28 Oct 2009; published 5 Nov 2009

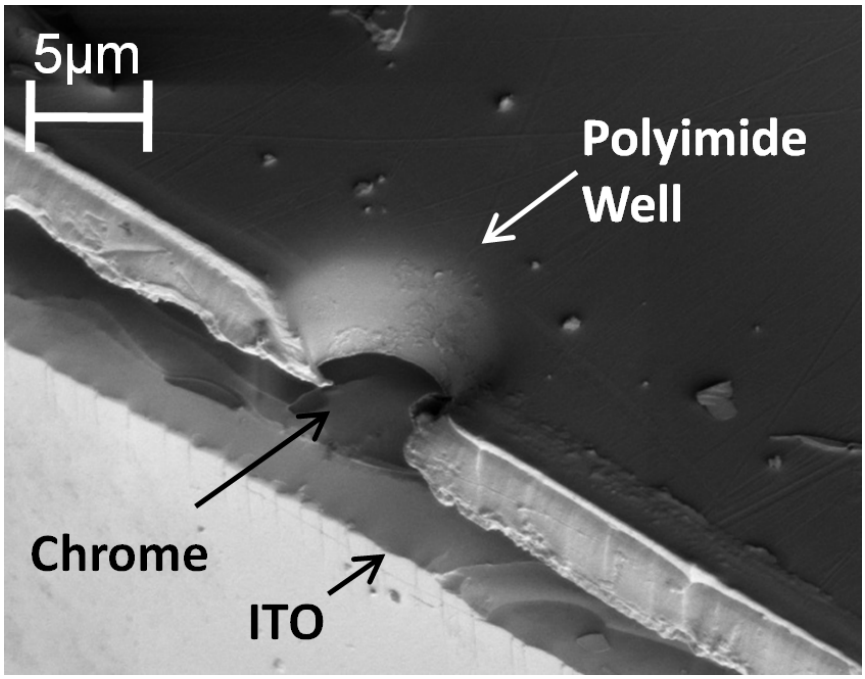

Fig. 11. SEM of the cross section of the electroactive microwell geometry previous to chrome layer etching. This alternative method is chosen due to ease of use and reduction of fabrication steps.

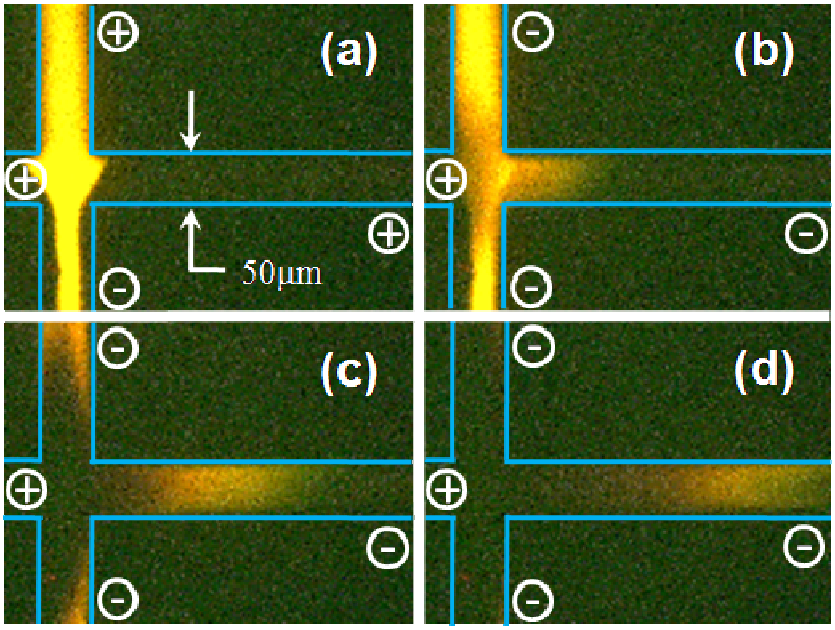

Fig. 12. Homogeneous data packet is being separated into its constituent red, yellow and green colors using capillary electrophoresis. Smaller sized quantum dots migrate faster downstream than the larger ones, suggesting that after bit erasure one could separate a data packet into its fundamental parts for reuse

#113847 - $15.00 USD Received 7 Jul 2009; revised 28 Oct 2009; accepted 28 Oct 2009; published 5 Nov 2009

Acknowledgments

This work is supported by National Science Foundation through the Sensors and Sensor Networks program under Grant No. NSF/CTS 0529045 and by the Defense Advanced Research Projects Agency through the Center for Optofluidic Integration funded under the University Photonics Research program.

#113847 - $15.00 USD Received 7 Jul 2009; revised 28 Oct 2009; accepted 28 Oct 2009; published 5 Nov 2009